Progress In Electromagnetics Research, Vol. 165, 93–105, 2019

A Physical Patch Model for GNSS-R Land Applications

Jiyue Zhu, Leung Tsang*, and Haokui Xu

Abstract—We consider the Global Navigation Satellite System Reflectometry (GNSS-R) for land applications. A distinct feature of land is that the topography has multiple elevations. The rms of elevations is in meters causing random phases between different elevations, which affect the coherent wave that has definite phase and the Fresnel zone effects as shown previously by a Kirchhoff numerical simulator (KA simulator). In this paper, we develop a physical patch model that is computationally efficient. The entire area within the footprint is divided into patches. Each patch is small enough to satisfy the plane wave incidence and is large enough to ignore mutual wave interactions between patches. The bistatic scattering cross section of each patch for the coherent and incoherent field is computed. The bistatic cross section of plane wave incidence is obtained from lookup tables (LUTs) of the numerical 3D solution of Maxwell equations (NMM3D). The SWC represents the summation of weighted coherent fields over patches. The SWICI represents the summation of weighted incoherent intensities over patches. The formula of the received power is the sum of powers from the SWC and SWICI (the SWC/SWICI formula). The weighting factor of each patch is based on the geometry, spherical waves, and the considerations of field amplitudes and phase variations. We also present an alternative formula, the "correlation" formula, using the summation of power from each physical area and correlations of SWCs from areas. The SWC/SWICI formula and the "correlation" formula are shown analytically to be the same. Results are compared with the KA simulator and two common models (the coherent model and the incoherent model). Results of the patch model are consistent with the KA simulator. For the simulation cases, the results fall between the coherent model and the incoherent model. The patch model is much more computationally efficient than the KA simulator and the results are more accurate. In examples of this paper, the patch model results are independent of patch size as long as the patch size smaller than 50 m and much larger than the wavelength of GNSS-R frequency.

1. INTRODUCTION

GNSS-R has been applied to remote sensing of the Earth including soil moisture [1–4], sea ice properties [5, 6], ocean surface wind speed [7, 8], snow water equivalent [9], etc. For land applications, GNSS-R receives specularly reflected GNSS signals, which are much stronger than backscattering even when there is attenuation by vegetation/forests. GNSS receivers at L-band include TechDemoSat-1 [2, 6] and CYGNSS [1, 3, 4, 7, 8]. There are also geostationary Mobile Use Objective System (MUOS) communication satellites, operating with dual-frequency channels at P-band (360–380 MHz and 240–270 MHz) [9]. GNSS-R is distinct from radar backscattering. In radar backscattering, scattered signals are dominated by incoherent contributions. However, the received signals of GNSS-R are in the specular direction and both coherent and incoherent waves contribute.

For electromagnetic wave scattering by random rough surfaces, the geometry of past rough surface problems is the rough surface with single elevation. For GNSS-R, microwave roughness (centimeter

Received 10 March 2019, Accepted 11 August 2019, Scheduled 15 August 2019
* Corresponding author: Leung Tsang (leutsang@umich.edu).
The authors are with the Radiation Laboratory, Department of Electrical Engineering and Computer Science, The University of Michigan, Ann Arbor, MI 48109-2122, USA.

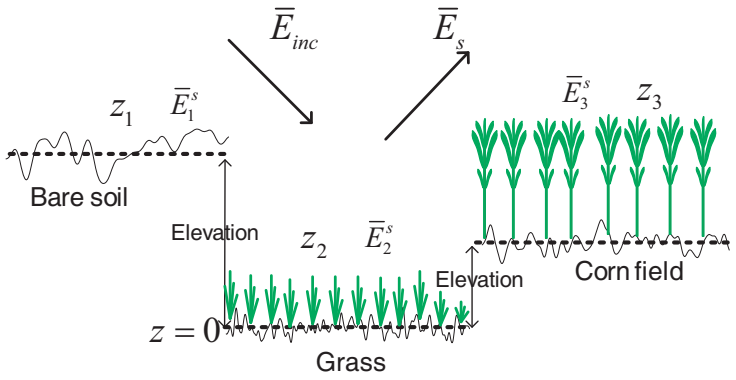

Figure 1. Land surface modeled by rough surfaces with multiple elevations.

scale) of the land surface is superimposed on the topography of multiple elevations, as shown in Figure 1. Furthermore, there are heterogeneities in the footprint. Within the tens of kilometer footprint, there can be bare soil, grass, corn fields, etc. The rms of elevations is in meters which is many times larger than the microwave wavelength of GNSS creating random phases between two different elevations. The two common models of GNSS-R are the coherent model [2, 3] and the incoherent model [4]. The coherent model ignores the incoherent fields and assumes the rough surface on a single elevation. As discussed in Gu's paper [1], there are regular alternate phase changes of π between adjacent Fresnel zones. The contributions of power mainly come from the first few Fresnel zones. However, the assumption of a single elevation is not valid as land surfaces have many elevations as indicated by the digital elevation model (DEM) [1]. On the other hand, the incoherent model ignores contributions of coherent fields. The assumption of the incoherent model is, due to the topography or large rms height of elevations, that the coherent fields "cancel" each other and become much less than incoherent fields. There are large differences in received power ratio, as large as 35 dB, between the results of the coherent model and the incoherent model. Another major difference is that results of the coherent model depend on the rms height of the rough surface while the incoherent model depends on the rms slope as in usual incoherent bistatic radar. The comparisons of the coherent and incoherent models are shown in Table 1.

Recently we studied GNSS-R for land applications using the Kirchhoff (KA) numerical simulator [1].

Table 1. Comparison of the coherent model and the incoherent model.

	Coherent model	**Incoherent model**
Scattered field	coherent fields only	incoherent fields only
Received power within the first Fresnel zone	60 dB larger than the incoherent model	60 dB smaller than the coherent model
Received power ratio over the footprint	35 dB larger than the incoherent model	35 dB smaller than the coherent model
Dependence	rms height h	rms slope s
Dependence on frequency	strongly dependence $\exp(-4k^2h^2\cos^2\theta_i)$	no dependence or weak dependence
Phase	definite phase	random phase
Dependence on dielectric permittivity	reflectivity	reflectivity
Derivation	Ad-hoc, not Maxwell's equation	Ad-hoc, not Maxwell's equation

In the KA simulator, the Kirchhoff integral is carried out over a 10 km by 10 km footprint which is discretized into 2 cm by 2 cm patches. A total of 2.5×10^{11} patches are used. The patch size of 2 cm by 2 cm is used to keep track of the phase of the scattered field from each patch. Results of KA simulator show that the topography of multiple elevations causes phase variations. The regular Fresnel zones (concentric ellipses) are destroyed, as shown in Gu's paper [1], which means there are no longer alternate phases of π for Fresnel zones as phases become random due to multiple elevations. The power contributions are not limited to the first few Fresnel zones. As shown in Gu's paper [1], the results of the KA simulator differ by many decibels from those of both the coherent model and the incoherent model.

However, the KA simulator is computationally intensive because of the dense discretization (cm scale) and requires parallel computation. In this paper, we develop a physical patch model that is computationally efficient and accurate. In the patch model, the complex terrain is represented by patches. SWC represents the summation of weighted coherent fields over patches. SWICI represents the summation of weighted incoherent intensity over patches. SWC is a new term because although it is a sum of coherent fields, it may not have definite phase. Thus SWC cannot be labeled as "coherent component". On the other hand, SWC is not like the usual incoherent field as SWC depends on rms height, but not rms slope. The received power is the sum of the power of SWC and the power of SWICI. Because of plane wave incidence of each patch, the coherent and incoherent field for each patch are obtained from pre-built look-up tables (LUTs) calculated from the scattering theory. The LUTs relate various microwave roughness and vegetation/forests properties to the coherent and incoherent scattering amplitudes of each patch. The patch size is much larger than that of the KA simulator. A patch size of 30 meters is used for the examples in this paper. The LUTs are implemented with the numerical 3D solutions of Maxwell equations (NMM3D) in this paper [10–12]. In addition, an alternative formula, called the correlation formula, is also derived. In the correlation formula, patches can also be grouped into physical areas such as grass area, rock area, forest area, etc. For each area, we calculate the area SWC and SWICI. The received power is the summation of power from each physical area and correlations of SWCs from areas. Numerical results of the patch model are illustrated. The results are consistent with the KA simulator within a few decibels. Compared with the KA numerical simulator, the physical patch model is much more computationally efficient because of the much larger patch size and is more accurate because of the utilization of NMM3D for the scattering amplitude. The patch model is independent of patch size once it satisfies with patch size conditions.

The organization of the paper is as follow. In Section 2, we describe the physical patch model and its implementation with NMM3D. In Section 3, numerical results are illustrated.

2. PHYSICAL PATCH MODEL FOR GNSS-R LAND APPLICATIONS

2.1. Coherent and Incoherent Scattered Fields of a Single Patch

As shown in Figure 1 and Figure 4, consider a land surface with multiple elevations on which microwave rough surface is superimposed. Although we use the general name of land, sea ice and glaciers are also considered as special cases. The complex terrain is divided into N patches, which are labeled as $n = 1, 2, \ldots, N$. It is required that the surface properties of each patch are statistically homogenous. Each patch has to be at a single elevation. The patch size has to be small enough such that plane wave incidence holds. By satisfying these conditions, the coherent field and incoherent intensity of each patch can be obtained from LUTs computed by the scattering theory of random rough surfaces and from transmission and volume scattering effects of vegetation. In this paper, we use the scattering amplitude $\bar{K}(\hat{k}_i,\hat{k}_s)$ to account for microwave effects of microwave roughness and vegetation/forests of the patch, where $\hat{k}_i$ and $\hat{k}_s$ are the incident and observation direction. The average $\langle \bar{K}(\hat{k}_i, \hat{k}_s)\rangle$ and variances $\langle |\bar{K}(\hat{k}_i, \hat{k}_s) - \langle \bar{K}(\hat{k}_i, \hat{k}_s)\rangle|^2\rangle$ are respectively the coherent scattering field and incoherent scattering intensity. The general definition of $\bar{K}(\hat{k}_i,\hat{k}_s)$ is described in the appendix.

In the implementation of this paper, $\bar{K}(\hat{k}_i,\hat{k}_s)$ is calculated by NMM3D. The advantages of applying NMM3D are 1) it provides exact coherent and incoherent field solution of the rough surface and 2) scattering by the rough surface that has exponential correlation function can be computed by NMM3D. Multiple scattering is included in NMM3D and gives a larger coherent component than the Kirchhoff

approximation as predicted by the paper of DeSanto and Shisa [13]. We have previously computed and saved large amounts of NMM3D bi-static scattering datasets for rough surfaces with a wide range of parameters (frequency, roughness, soil moisture, and incident angles) for SMAP [11, 12, 14]. The patch model implemented with NMM3D shall be labeled as the patch/NMM3D model.

2.2. Weighted Coherent Field and Incoherent Intensity of a Single Patch

In the GNSS-R system, the transmitter and receiver are at positions, $\bar{r}_t$ and $\bar{r}_r$, respectively at a certain moment in time (for a single delay/Doppler bin) [15]. The incident wave is a spherical wave.

$$\bar{E}_{inc} = \bar{e}_i \sqrt{\frac{P_t \eta}{2\pi}} \frac{\exp(ikR_t)}{R_t} \tag{1}$$

where η and k are free space wave impedance and wavenumber. P_t is the transmitted power, and $\bar{e}_i$ is the polarization. For a point $\bar{r}$ on the surface, $R_t = |\bar{r} - \bar{r}_t|$ and $R_r = |\bar{r}_r - \bar{r}|$ are, respectively, distances to the transmitter and the receiver.

In the physical patch model, the patch size is small enough so that the entire patch is illuminated by a uniform plane wave. For a single patch, the weighted coherent scattered field of the nth patch is given by [16],

$$\left\langle \bar{E}_n^s(\bar{r}_r) \right\rangle = \sqrt{\frac{P_t \eta}{2\pi}} \frac{\operatorname{sinc}(k_{ndx} L_{nx}/2) \operatorname{sinc}(k_{ndy} L_{ny}/2)}{R_{nt} R_{nr}} \exp(ik(R_{nr} + R_{nt})) \left\langle \bar{K}_n\left(\hat{k}_{ni}, \hat{k}_{ns}\right) \right\rangle \tag{2}$$

where $\bar{r}_n$ is the center of the nth patch. $R_{rn} = |\bar{r}_r - \bar{r}_n|$ and $R_{tn} = |\bar{r}_n - \bar{r}_t|$. $\hat{k}_{ns} = \frac{\bar{r}_r - \bar{r}_n}{|\bar{r}_r - \bar{r}_n|}$ is the observation direction for the nth patch. $\hat{k}_{ni} = \frac{\bar{r}_n - \bar{r}_t}{|\bar{r}_n - \bar{r}_t|}$ is the incident direction for the nth patch. L_{nx} and L_{ny} are the size of the nth patch in x and y directions. The wave vector difference is $\bar{k}_{nd} = k_{ndx}\hat{x} + k_{ndy}\hat{y} + k_{ndz}\hat{z} = \hat{k}_{ns} - \hat{k}_{ni}$. There are three terms in the equation of the weighted coherent field of the nth patch. The term $\exp(ik(R_{nr} + R_{nt}))$ is the phase at the center of the nth patch so that the phase is highly dependent on the center location of the patch. The term $\operatorname{sinc}(\frac{k_{ndx} L_{nx}}{2}) \operatorname{sinc}(\frac{k_{ndy} L_{ny}}{2})$ is the amplitude which represents the sharp peak in the specular direction of the coherent field [16]. The term $\frac{1}{R_{nt} R_{nr}}$ is the amplitude decay caused by the propagation distance for spherical waves. The weighted coherent field is proportional to the area of the patch.

The weighted incoherent intensity of the nth patch is given by

$$I_n^{ICI}(\bar{r}_r) = \frac{P_t \eta}{2\pi (R_{nt} R_{nr})^2} \left\langle \left| \bar{K}_n\left(\hat{k}_{ni}, \hat{k}_{ns}\right) - \left\langle \bar{K}_n\left(\hat{k}_{ni}, \hat{k}_{ns}\right) \right\rangle \right|^2 \right\rangle \tag{3}$$

Key ideas in the physical patch model are as follows.

a) The coherent scattering amplitude $\langle \bar{K}_n(\hat{k}_{ni}, \hat{k}_{ns}) \rangle$ and the incoherent amplitude $\langle |\bar{K}_n(\hat{k}_{ni}, \hat{k}_{ns}) - \langle \bar{K}_n(\hat{k}_{ni}, \hat{k}_{ns}) \rangle|^2 \rangle$ represent microwave effects of the rough surface and vegetation/forest from the nth patch.

b) We use the Kirchhoff concept to represent the phase and amplitude due to spherical waves. The phase term $\exp(ik(R_{nr} + R_{nt}))$ and amplitude term $\frac{\operatorname{sinc}(\frac{k_{ndx} L_{nx}}{2}) \operatorname{sinc}(\frac{k_{ndy} L_{ny}}{2})}{R_{nt} R_{nr}}$ depend on the patch elevation and position.

Based on the analysis above, we summarize below the requirements for the patch size. For a single patch, it is required that the patch size A is

a) Not too big.
   i. Be single elevation.
   ii. Satisfies plane wave incidence.
   iii. Be less than Fresnel zone size to keep a constant phase of the incident/scattered wave over the patch.

b) Not too small.
   i. Be much larger than wavelength to have a dominant specular reflection.
   ii. Be large enough to ignore mutual wave interactions between patches.

2.3. SWC and SWICI in Summation over Patches

For summation over N patches, the SWC is given by summation of weighted coherent fields

$$\bar{E}^{SWC}(\bar{r}_r) = \sqrt{\frac{P_t\eta}{2\pi}} \sum_{n=1}^{N} \frac{\operatorname{sinc}(k_{ndx}L_{nx}/2)\operatorname{sinc}(k_{ndy}L_{ny}/2)}{R_{nt}R_{nr}} \exp(ik(R_{nr}+R_{nt})) \left\langle \bar{K}_n\left(\hat{k}_{ni},\hat{k}_{ns}\right)\right\rangle \quad (4)$$

and the SWICI is the summation of weighted incoherent intensities

$$I^{SWICI}(\bar{r}_r) = \frac{P_t\eta}{2\pi} \sum_{n=1}^{N} \frac{1}{(R_{nt}R_{nr})^2} \left\langle \left| \bar{K}_n\left(\hat{k}_{ni},\hat{k}_{ns}\right) - \left\langle \bar{K}_n\left(\hat{k}_{ni},\hat{k}_{ns}\right)\right\rangle \right|^2 \right\rangle \quad (5)$$

It is clear that the variation of the weighted coherent field over patches is much more rapid than that of the weighted incoherent intensity. For the weighted incoherent intensity, the bistatic scattering coefficient $\langle|\bar{K}_n(\hat{k}_{ni},\hat{k}_{ns}) - \langle\bar{K}_n(\hat{k}_{ni},\hat{k}_{ns})\rangle|^2\rangle$ only changes when surface roughness or vegetation canopy changes. The SWICI is similar to incoherent addition as in incoherent radar bistatic scattering.

For the SWC, the variation of the weighted coherent field over patches is as follows.

a) The amplitude of $\langle\bar{K}_n(\hat{k}_{ni},\hat{k}_{ns})\rangle$ varies slowly over the footprint as well as the phase of $\langle\bar{K}_n(\hat{k}_{ni},\hat{k}_{ns})\rangle$.

b) The more rapid variations are due to the phase of the spherical waves, $\exp(ik(R_{nr}+R_{nt}))$. The variations of phase are due to (i) vertical elevations in topography, and (ii) the phase change of spherical wave by the change of the horizontal position of the patch.

c) At the periphery of the 10 km by 10 km footprint, the phase change is rapid for the spherical waves. One may need small patch to keep track of the phase. However, when there are rapid variations in the coherent field phase the contribution to the SWC is small. In the examples of this paper, there is a circle with 8 km radius (shown in Figure 2). Outside the circle, the contributions of coherent fields to SWC are small due to rapid phase variations of the coherent field.

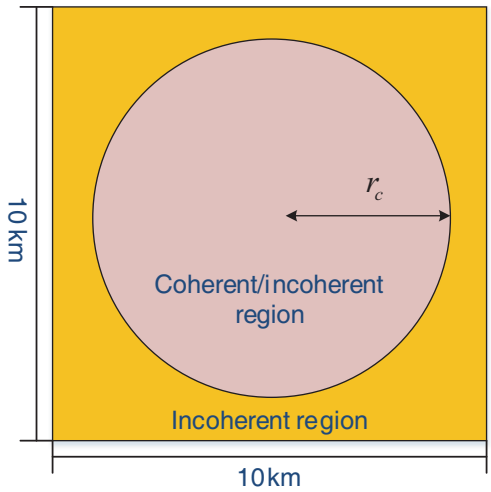

Figure 2. Simulated area divided into the coherent/incoherent region and the incoherent region.

In Table 2, we compare the SWC and SWICI with the coherent field and incoherent field. The power of the SWC and coherent field both depend on the rms height of the surface. While the incoherent intensity and the SWICI depend on the rms slope. However, the SWC, though a summation of coherent fields, should not be labeled as "coherent component" as its phase can be random if there are many patches with variations of phases from patch to patch. The phase of the SWC can be definite, quasi-definite or random depending on the number of patches that contribute. If the SWC is dominated by a few patches within the area, the phase is definite. If the SWC is contributed from thousands of patches,

Table 2. Comparison of the coherent field, incoherent intensity, SWC and SWICI.

	The coherent field	**The incoherent intensity**	**The SWC (multiple elevations)**	**The SWICI (multiple elevations)**
Phase	definite phase	incoherent field has random phase	definite, quasi-definite, or random	incoherent field has random phase
Power vs. surface para.	rms height h	rms slope s	rms height h	rms slope s
Power vs. area	Proportional to area square	Proportional to area	Case by case basis	Proportional to area

the phase is random. Therefore, the SWC is conceptually a new quantity. On the other hand, the SWICI is similar to the incoherent intensity. The received power of the area depends on rms height if the SWC dominates. The received power depends on rms slope if the SWICI dominates.

The received power is the sum of the power of SWC and the power from SWICI given as follow

$$\left\langle \left|\bar{E}_s\right|^2 \right\rangle = \left|\bar{E}^{SWC}\right|^2 + I^{SWICI} \tag{6}$$

where $\bar{E}_s$ is the total scattered field of the footprint. $\bar{E}^{SWC} = \langle \bar{E}_s \rangle$ and $|\bar{E}^{SWC}|^2$ is the power of SWC. Equation (6) is denoted as the SWC/SWICI formula.

2.4. The Correlation Formula

Patches can be grouped based on their physical properties to form physical areas. Let the footprint be composed of physical areas such as grass areas, forest areas, bare soil areas, rock areas, as shown in Figure 4. Note each area does not have to be homogeneous. The only requirement is that each patch is homogeneous. Each area usually has multiple elevations. Let i be the area index, and there are M areas with $i = 1, 2, \ldots, M$. The scattered field from the ith area is $\bar{E}_i^s$. The scattered field received by the receiver is

$$\bar{E}_s = \sum_{i=1}^{M} \bar{E}_i^s \tag{7}$$

Take absolute valued square and then take average

$$\left\langle \left|\bar{E}_s\right|^2 \right\rangle = \sum_{i=1}^{M} \left\langle \left|\bar{E}_i^s\right|^2 \right\rangle + \sum_{i=1}^{M} \sum_{j=1, i\neq j}^{M} \langle \bar{E}_i^s \bar{E}_j^{s*} \rangle \tag{8}$$

where the angular bracket $\langle\ \rangle$ means average. We next ignore correlation of incoherent fields. Then

$$\left\langle \left|\bar{E}_s\right|^2 \right\rangle = \sum_{i=1}^{M} \left\langle \left|\bar{E}_i^s\right|^2 \right\rangle + \sum_{i=1}^{M} \sum_{j=1, i\neq j}^{M} \langle \bar{E}_i^s \rangle \langle \bar{E}_j^{s*} \rangle \tag{9}$$

The above equation is labeled as the correlation formula. There are two terms contributing to the total power. The first term is the scattered power from each area. The second term is the correlation of average fields from different areas. Next we compute $\langle \bar{E}_i^s \rangle$ and $\langle |\bar{E}_i^s|^2 \rangle$ in terms of SWC and SWICI of the area. Let each area i be composed of N_i patches. Then the summation of N_i gives N which is the total number of patches as in Section 2.2, $N = \sum_{i=1}^{M} N_i$. The SWC of the ith area is

$$\langle \bar{E}_i^s \rangle = \bar{E}_i^{SWC} = \sum_{n_i=1}^{N_i} \langle \bar{E}_{n_i}^s \rangle \tag{10}$$

where $\langle \bar{E}^s_{n_i} \rangle$ is the weighted coherent field of the patch as given in Equation (2). The scattered power of the ith area is the sum of SWC and SWICI of the area.

$$\left\langle \left| \bar{E}^s_i \right|^2 \right\rangle = \left| \bar{E}^{SWC}_i \right|^2 + I^{SWICI}_i \tag{11}$$

where the SWICI of the ith area is

$$I^{SWICI}_i = \sum_{n_i=1}^{N_i} I^{ICI}_{n_i} \tag{12}$$

$I^{ICI}_{n_i}$ is the weighted incoherent intensity of the patch as given in Equation (3). The correlation formula becomes

$$\left\langle \left| \bar{E}_s \right|^2 \right\rangle = \sum_{i=1}^{M} \left\langle \left| \bar{E}^s_i \right|^2 \right\rangle + \sum_{i=1}^{M} \sum_{j=i+1}^{M} 2Re \left(\bar{E}^{SWC}_i \bar{E}^{SWC*}_j \right) \tag{13}$$

The first term is the sum of powers of both SWC and SWICI from each area. This is different from the coherent model which includes coherent waves only and also different from the incoherent model that only includes the incoherent waves. In the second term, correlations of SWCs between two different areas are taken into account. In the appendix, we show that the correlation formula and the SWC/SWICI formula are equivalent. The patch model is not dependent on how the areas are divided as different schemes will give consistent results as the correlation term will make up for different schemes.

3. RESULTS AND DISCUSSION

Three examples will be shown: 1) a land surface of bare soil with the topography of multiple elevations, 2) a heterogeneous land surface with one area dominating and 3) a heterogeneous land surface consists of multiple areas with multiple elevations.

The configuration is as follows [1]. The frequency is 1.575 GHz. The height of the transmitter is $h_t = 2.02 \times 10^7$ m and the receiver is at height of $h_r = 5 \times 10^5$ m. The gain for transmitted and received antenna are 13 dB and 14 dB separately. The horizontal distance between two antennas is 1.7369×10^7 m. The specular point at $z = 0$ plane is set as the coordinate origin $(x, y) = (0, 0)$. The xz plane contains both the transmitter and the receiver. The simulated area is 10 km by 10 km. The vegetation or forest layer effects are taken into account by the transmission coefficient which is obtained from the baseline SMAP active retrieval algorithm [16, 17].

3.1. Physical Patch/NMM3D Model with Patches of 30 m by 30 m

The simulation area is a bare soil surface with multiple elevations. The permittivity of the land is $\varepsilon_{soil}=(5.5 + 2i)\varepsilon_0$. The elevations of the land surface are from the digital elevation model (DEM). The DEM data are from Advanced Space borne Thermal Emission and Reflection Radiometer (ASTER) Global Digital Elevation Model version 2 (GDEM2) [1]. The ASTER GDEM2 is released by NASA and METI Japan in mid-October 2011, which covers the land between 83°N and 83°S using 22702 $1^\circ \times 1^\circ$ tiles. Each $1^\circ \times 1^\circ$ tile is comprised of 3601 by 3601 pixels with a resolution of 30 m by 30 m at the equator. The chosen area is from Georgia, USA with the coordinate of 31°49′50″N and 83°49′50″W. In physical patch/NMM3D model, the exponential correlation function is used. In the KA simulator and the incoherent model, the Gaussian correlation function is used.

The received power ratio of HH-polarization as a function of rms height is shown in Figure 3 and Table 3. Compared with the coherent model results, both KA simulator and patch/NMM3D model results are smaller. They are consistent within a few decibels. For larger rms heights, the difference between the patch/NMM3D model and KA simulator becomes larger because multiple scattering is included in NMM3D. This result is consistent with the study of coherent wave amplitude in the past that shows coherent wave amplitude is larger than that predicted by the Kirchhoff approximation [11, 13]. In Table 4, the patch model is compared with KA simulator.

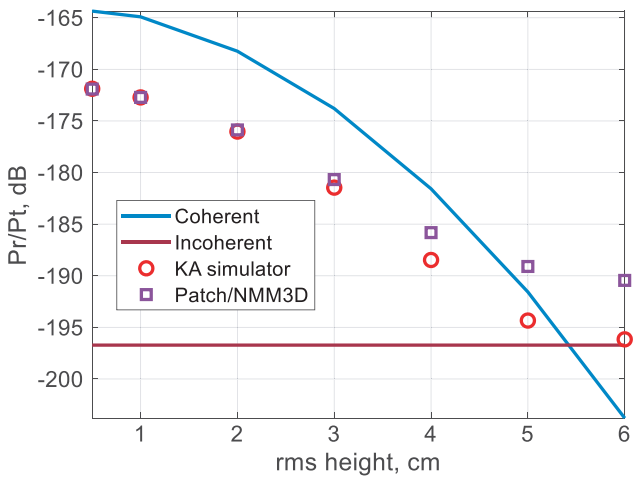

Figure 3. Received power ratio P_r/P_t as a function of rms height.

Table 3. Comparison of received power ratio among models.

HH P_r/P_t dB	**rms height**				
	h = 2 cm	**h = 3 cm**	**h = 4 cm**	**h = 5 cm**	**h = 6 cm**
KA simulator, 2 cm by 2 cm patch	−176.03	−181.46	−188.47	−194.34	−196.16
Patch/NMM3D, 30 m by 30 m patch	−175.87	−180.68	−185.82	−189.10	−190.45

Table 4. Comparison of KA simulator and patch model.

	KA simulator	**Patch model**
Discretization	2 cm by 2 cm	Much bigger (30 m by 30 m in this paper)
Efficiency	40 hour (20 cores)	1 second (1 core)
Accuracy	Kirchhoff approximation	Scattering theory (NMM3D look-up table)
Surface type	Only Gaussian	Gaussian and exponential

3.2. The Land Surface with One Dominating Area

In Figure 4(a), we show a land surface which is divided into soil and forest area. The soil area is located at the center and has only one elevation of 20.2 m with small rms height. The forest area has multiple elevations with large rms height. The mean elevation H_m for forest area is 30.32 m. To create multiple elevations for the forest area, a random number is added to the mean elevation for each 270 m by 270 m, that is $H_{DEM}(x, y) = H_m + 0.5\delta_r H_m$. The random number is of uniform distribution between zero and 50% of the mean elevation $\delta_r \in [0, 1]$. The transmission for the forest is 0.45 [17]. The SWC of the forest area is small due to the large rms height and multiple elevations. Table 5 shows that the SWC from the soil area dominates the total SWC. The total SWC has a definite phase and is coherent. The calculated P_r/P_t is −161.90 dB with −161.90 dB contribution from the SWC and −208.56 dB contribution from the SWICI. The P_r/P_t has dominated contribution from the soil area.

3.3. The Land Surface with Multiple Areas and Multiple Elevations

In Figure 4(b), we show a land surface that consists of grass, rock, bare soil, and forest. The land surface is divided into 5 areas with multiple elevations for each area. The mean elevation H_m for the rock, bare soil, forest1, grass and forest2 area are 18.32 m, 10.2 m, 10.6 m, 15.5 m and 33.23 m. To

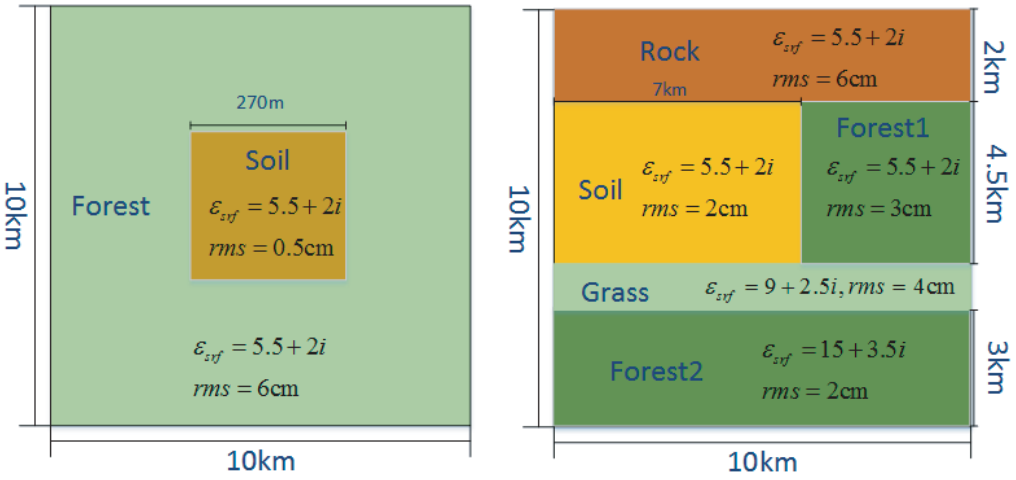

Figure 4. Land surface divided into physical areas: (a) the second example in 3.2 and (b) the third example in 3.3.

Table 5. The amplitude and phase of SWCs in the second example.

	SWC of soil	**SWC of forest**	**Total SWC**
Amplitude (V/m)	8.273×10^{-7}	0.093×10^{-7}	8.200×10^{-7}
Phase (rad)	-2.528	-0.047	-2.521

Table 6. Contributions of terms in patch model for the SWC+SWICI formula.

Model		$\mathbf{P_r/P_t}$ **dB**
The coherent model		-168.24 dB
The incoherent model		-197.96 dB
KA simulator		-183.65 dB
The patch/NMM3D model	SWC	-181.99 dB
	SWICI	-201.31 dB
	Total	$\mathbf{-181.94\,dB}$

create multiple elevations for each area, we generate random elevations for every 90 m by 90 m area with the same method used in the second example. The transmission for the grass is 0.69 and for the forest is 0.45 [17]. The soil and forest2 area are with small rms height. The bare soil, grass and forest2 area are with a large area. These three areas dominate the received power. The rock area has only SWICI contributions. Other areas have both SWC and SWICI contributions. In Table 6 and Table 7, the contributions for Equations (6) and (13) are listed, respectively. The results of the patch model are consistent with KA simulator and are about 2 dB higher. Table 6 indicates that P_r/P_t is dominated by the SWC. The SWICI component of the patch model is smaller than results of the incoherent model. This is because the exponential correlation function is used in the patch model while the Gaussian correlation function is used in the incoherent model. In Table 7, the results using the correlation formula are shown. The table shows values of negative correlations that reduce the total power received.

Table 7. Contributions of terms in patch model for the correlation formula.

$\langle\lvert\bar{E}_i\rvert^2\rangle$	**Power of each area**	$2\mathrm{Re}(\bar{E}_i^{SWC}\bar{E}_j^{SWC*})$	**Correlations of SWC**	$\mathbf{P_r/P_t}$ **dB**
Bare soil	5.429×10^{-15}	Bare soil & Grass	0.416×10^{-15}	
Forest2	0.415×10^{-15}	Bare soil & Forest2	-1.429×10^{-15}	
Grass	0.486×10^{-16}	Grass & Forest2	0.723×10^{-15}	
Total	6.330×10^{-15}	Total	-0.287×10^{-15}	$\mathbf{-181.94\,dB}$
KA simulator				183.65 dB
The coherent model				−168.24 dB
The incoherent model				−197.96 dB

3.4. Convergence of the Patch Model with Patch Size

In this paper, the received power ratio is calculated by using a patch size of 30 m by 30 m. Different patch sizes are applied to the example in Section 3.3. Figure 5 illustrates the received power ratio calculated as a function of patch size. The results show convergence for patch size less than 50 m. For patch size smaller than 50 m, the results oscillate around −181.95 dB within about 0.1 dB. Therefore, the choice of 30 m patch size gives accurate results for the examples in this paper.

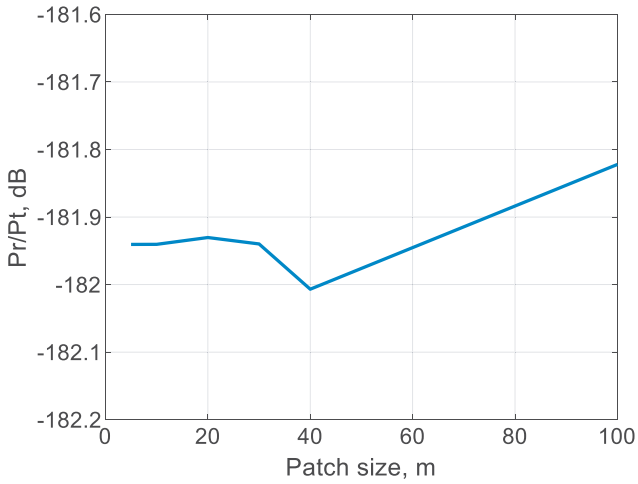

Figure 5. Convergence of the patch/NMM3D model with patch size.

4. CONCLUSIONS

A patch model for GNSS-R land applications is proposed. The topography of multiple elevations is accounted for. The land surface is divided into patches. The coherent and incoherent scattering amplitudes of each patch can be calculated from scattering theory because the patch is small enough so that the incident wave is a plane wave. Compared with the KA simulator, the physical patch model is much more computationally efficient because of the much larger patch size and is more accurate because of the use of NMM3D. The received power is the sum of the power of SWC and the power of SWICI. If SWC is larger than SWICI, the received power ratio depends on rms height. If SWICI is larger than SWC, the received power ratio depends on the slope of the surface. We have not considered water bodies. Water bodies are patches with small rms height and single elevations. The effects are well known and can be readily incorporated in the physical patch model. In the future, the NMM3D for vegetation/forests [18] and terrestrial snow [19, 20] can also be applied.

APPENDIX A.

A.1. Definition of the Scattering Amplitude $\bar{K}(\hat{k}_i,\hat{k}_s)$

Consider the incident wave with the electric field $\bar{E}_i$. Define the horizontal polarization direction $\hat{h}_i = \frac{\hat{z}\times\hat{k}_i}{|\hat{z}\times\hat{k}_i|}$ and the vertical polarization $\hat{v}_i = \hat{h}_i \times \hat{k}_i$. Then

$$\bar{E}_i = \left(\hat{v}_i E_{vi} + \hat{h}_i E_{hi}\right) \exp\left(i\bar{k}_i \cdot \bar{r}\right) \tag{A1}$$

where $\bar{k}_i = k\hat{k}_i$. Similarly for the scattering field, we have the observation direction $\hat{k}_s$. The horizontal polarization is $\hat{h}_s = \frac{\hat{z}\times\hat{k}_s}{|\hat{z}\times\hat{k}_s|}$, and the vertical polarization is $\hat{v}_s = \hat{h}_s \times \hat{k}_s$. The scattered field is expressed by

$$\bar{E}_s = \left(\hat{v}_s E_{vs} + \hat{h}_s E_{hs}\right) \frac{\exp(ikr)}{r} \tag{A2}$$

The scattering amplitude matrix relates the incident wave and scattered wave as

$$\begin{bmatrix} E_{vs} \\ E_{hs} \end{bmatrix} = \begin{bmatrix} f_{vv}\left(\hat{k}_i,\hat{k}_s\right) & f_{vh}\left(\hat{k}_i,\hat{k}_s\right) \\ f_{hv}\left(\hat{k}_i,\hat{k}_s\right) & f_{hh}\left(\hat{k}_i,\hat{k}_s\right) \end{bmatrix} \begin{bmatrix} E_{vi} \\ E_{hi} \end{bmatrix} \tag{A3}$$

The scattering amplitude matrix is

$$\bar{\bar{K}}\left(\hat{k}_i,\hat{k}_s\right) = \begin{bmatrix} f_{vv}\left(\hat{k}_i,\hat{k}_s\right) & f_{vh}\left(\hat{k}_i,\hat{k}_s\right) \\ f_{hv}\left(\hat{k}_i,\hat{k}_s\right) & f_{hh}\left(\hat{k}_i,\hat{k}_s\right) \end{bmatrix} \tag{A4}$$

In this paper, we let the polarization of the incident wave be $\bar{e}_i$, the scattering amplitude $\bar{K}(\hat{k}_i,\hat{k}_s)$ is defined as

$$\bar{K}\left(\hat{k}_i,\hat{k}_s\right) = \bar{\bar{K}}\left(\hat{k}_i,\hat{k}_s\right) \cdot \bar{e}_i \tag{A5}$$

If $|E_{vi}| = |E_{hi}|$, $\frac{E_{hi}}{E_{vi}} = i$ or $-i$ corresponds to the left- and right-handed circular polarizations of the incident wave, respectively. If $|E_{vs}| = |E_{hs}|$, $\frac{E_{hs}}{E_{vs}} = i$ or $-i$ corresponds to the left- and right-handed circular polarizations of the scattered wave, respectively.

A.2. Equivalence of the SWC/SWICI Formula and the Correlation Formula

To show the equivalence, we start with the correlation formula. Substitute Equation (11) into (13)

$$\left\langle \left|\bar{E}_s\right|^2 \right\rangle = \sum_{i=1}^{M} \left(\left|\bar{E}_i^{SWC}\right|^2 + I_i^{SWICI} \right) + \sum_{i=1}^{M} \sum_{j=i+1}^{M} 2Re\left(\bar{E}_i^{SWC} \bar{E}_j^{SWC*}\right) \tag{A6}$$

Next, put the SWC terms together

$$\left\langle \left|\bar{E}_s\right|^2 \right\rangle = \left| \sum_{i=1}^{M} \bar{E}_i^{SWC} \right|^2 + \sum_{i=1}^{M} I_i^{SWICI} \tag{A7}$$

Substitute Equations (10) and (12) into the formula above. The SWC and SWICI of the ith area are expressed by the summation of coherent fields and incoherent intensities respectively of N_i patches

$$\left\langle \left|\bar{E}_s\right|^2 \right\rangle = \left| \sum_{i=1}^{M} \sum_{n_i=1}^{N_i} \left\langle \bar{E}_{n_i}^{s} \right\rangle \right|^2 + \sum_{i=1}^{M} \sum_{n_i=1}^{N_i} I_{n_i}^{ICI} \tag{A8}$$

We relabel the patches by $n= 1, 2, \ldots, N$. Then

$$\begin{aligned} \sum_{i=1}^{M}\sum_{n_i=1}^{N_i}\langle \bar{E}_{n_i}^{s}\rangle &= \sum_{n=1}^{N}\langle \bar{E}_{n}^{s}\rangle = \bar{E}^{SWC} \\ \sum_{i=1}^{M}\sum_{n_i=1}^{N_i} I_{n_i}^{ICI} &= \sum_{n=1}^{N} I_{n}^{ICI} = I^{SWICI} \end{aligned} \tag{A9}$$

Thus, we get the SWC/SWICI formula

$$\left\langle \left|\bar{E}_s\right|^2 \right\rangle = \left|\bar{E}^{SWC}\right|^2 + I^{SWICI} \tag{A10}$$

Therefore, the correlation formula and the SWC/SWICI formula are equivalent based on the analytical derivations above.

REFERENCES

1. Gu, W., H. Xu, and L. Tsang, "A numerical Kirchhoff simulator for GNSS land applications," *Progress In Electromagnetics Research*, Vol. 164, 119–133, 2019.
2. Chew, C., R. Shah, C. Zuffada, G. Hajj, D. Masters, and A. J. Mannucci, "Demonstrating soil moisture remote sensing with observations from the UK TechDemoSat-1 satellite mission," *Geophysical Research Letters*, Vol. 43, No. 7, 3317–3324, 2016.
3. Kim, H. and V. Lakshmi, "Use of Cyclone Global Navigation Satellite System (CYGNSS) observations for estimation of soil moisture," *Geophysical Research Letters*, Vol. 45, No. 16, 8272–8282, 2018.
4. Al-Khaldi, M., J. Johnson, A. O'Brien, F. Mattia, and A. Balenzano, "GNSS-R time-series soil moisture retrievals from vegetated surfaces," *IGARSS 2018 — 2018 IEEE International Geoscience and Remote Sensing Symposium*, 2035–2038, 2018.
5. Cardellach, E., F. Fabra, O. Nogués-Correig, S. Oliveras, S. Ribó, and A. Rius, "GNSS-R ground-based and airborne campaigns for ocean, land, ice and snow techniques: Application to the GOLD-RTR datasets," *Radio Sci.*, Vol. 46, 2011.
6. Li, W., E. Cardellach, F. Fabra, A. Rius, S. Ribó, and M. Martín-Neira, "First spaceborne phase altimetry over sea ice using TechDemoSat-1 GNSS-R signals," *Geophys. Res. Lett.*, Vol. 44, 2017.
7. Clarizia, M. P. and C. S. Ruf, "Bayesian wind speed estimation conditioned on significant wave height for GNSS-R ocean observations," *J. Atmos. Oceanic Technol.*, Vol. 34, 1193–1202, 2017.
8. Ruf, C., S. Gleason, and D. S. McKague, "Assessment of CYGNSS wind speed retrieval uncertainty," *IEEE J. Sel. Topics Appl. Earth Obs. Remote Sens.*, Vol. 12, No. 1, 87–97, Jan. 2019.
9. Yueh, S., X. Xu, R. Shah, Y. Kim, J. L. Garrison, A. Komanduru, and K. Elder, "Remote sensing of snow water equivalent using coherent reflection from satellite signals of opportunity: Theoretical modeling," *IEEE Journal of Selected Topics in Applied Earth Observations and Remote Sensing*, Vol. 10, No. 12, 5529–5540, 2017.
10. Tsang, L., J. Zhu, Y. Du, and R. Gao, "Electromagnetic scattering model for GNSS-R land applications including effects of multiple elevations in random rough surfaces," *IEEE GNSS+R 2019*, Benevento, Italy, May 20–22, 2019.
11. Huang, S. L. Tsang, E. G. Njoku, and K. S. Chen, "Backscattering coefficients, coherent reflectivities, and emissivities of randomly rough soil surfaces at L-band for SMAP applications based on numerical solutions of Maxwell equations in three-dimensional simulations," *IEEE Trans. Geoscience and Remote Sensing*, Vol. 48, 2557–2568, 2010.
12. Liao, T.-H., L. Tsang, S. Huang, N. Niamsuwan, S. Jaruwatanadilok, S. B. Kim, et al., "Copolarized and cross-polarized backscattering from random rough soil surfaces from L-band to Ku-band using numerical solutions of Maxwell's equations with near-field precondition," *IEEE Trans. Geoscience and Remote Sensing*, Vol. 54, 651–662, 2016.

13. DeSanto, J. A. and O. Shisha, "Numerical solution of a singular integral equation in random rough surface scattering theory," *Journal of Computational Physics*, Vol. 15, No. 2, 286–292, 1974.
14. Kim, S.-B., J. J. Van Zyl, J. T. Johnson, M. Moghaddam, L. Tsang, A. Colliander, et al., "Surface soil moisture retrieval using the L-band synthetic aperture radar onboard the soil moisture active-passive satellite and evaluation at core validation sites," *IEEE Trans. Geoscience and Remote Sensing*, Vol. 55, 1897–1914, 2017.
15. Gleason, S., "Level 1B DDM calibration algorithm theoretical basis document," CYGNSS Project Document 148-0137, Rev 2, Aug. 20, 2018.
16. Tsang, L. and J. Kong, *Scattering of Electromagnetic Waves, Vol. 3: Advanced Topics*, Wiley Interscience, 2001.
17. Jackson, T. J. and T. J. Schmugge, "Vegetation effects on the microwave emission of soils," *Remote Sensing of Environment*, Vol. 36, No. 3, 203–212, 1991.
18. Huang, H., L. Tsang, E.G. Njoku, A. Colliander, T.-H. Liao, and K.-H. Ding, "Propagation and scattering by a layer of randomly distributed dielectric cylinders using monte carlo simulations of 3D Maxwell equations with applications in microwave interactions with vegetation," *IEEE Access*, Vol. 5, 11985–12003, 2017.
19. Tan, S., J. Zhu, L. Tsang, and S. V. Nghiem, "Microwave signatures of snow cover using numerical Maxwell equations based on discrete dipole approximation in bicontinuous media and half-space dyadic Green's function," *IEEE J. Sel. Topics Appl. Earth Observ. Remote Sens.*, Vol. 10, No. 11, 4686—4702, Nov. 2017.
20. Tsang, L. and J. Kong, *Scattering of Electromagnetic Waves, Vol. 1: Theories and Applications*, Wiley Interscience, 2001.